Landau quantization near generalized Van Hove singularities
Magnetic breakdown and orbit networks

Zakharov, V. A.; Bozkurt, A. Mert; Akhmerov, A. R.; Oriekhov, D. O.

DOI
10.1103/PhysRevB.109.L081103

Publication date
2024

Document Version
Final published version

Published in
Physical Review B

Letter | Editors' Suggestion

Landau quantization near generalized Van Hove singularities: Magnetic breakdown and orbit networks

V. A. Zakharov [1], A. Mert Bozkurt [2,3], A. R. Akhmerov [2], and D. O. Oriekhov [1]

[1] *Instituut-Lorentz, Universiteit Leiden, P.O. Box 9506, 2300 RA Leiden, The Netherlands*

[2] *Kavli Institute of Nanoscience, Delft University of Technology, Delft 2600 GA, The Netherlands*

[3] *QuTech, Delft University of Technology, Delft 2600 GA, The Netherlands*

(Received 22 April 2023; revised 22 September 2023; accepted 18 January 2024; published 5 February 2024)

We develop a theory of magnetic breakdown (MB) near high-order saddle points in the dispersions of two-dimensional materials, where two or more semiclassical cyclotron orbits approach each other. MB occurs due to quantum tunneling between several trajectories, which leads to nontrivial scattering amplitudes and phases. We show that for any saddle point this problem can be solved by mapping it to a scattering problem in a 1D tight-binding chain. Moreover, the occurrence of magnetic breakdown on the edges of the Brillouin zone facilitates the delocalization of the bulk Landau level states and the formation of 2D orbit networks. These extended network states compose dispersive mini bands with finite energy broadening. This effect can be observed in transport experiments as a strong enhancement of the longitudinal bulk conductance in a quantum Hall bar. In addition, it may be probed in STM experiments by visualizing bulk current patterns.

DOI: 10.1103/PhysRevB.109.L081103

Magnetic breakdown (MB) in a single Bloch band occurs when two semiclassical trajectories of quasiparticles come close to each other and quantum tunneling between them becomes possible. This situation naturally appears near usual saddle points that give rise to logarithmic van Hove singularities in the density of states [1]. In novel atomically thin 2D materials a new family of saddle points arises, around which the dispersion is flatter than in the usual case. This leads to power-law divergences in the density of states known as high-order van Hove singularities [2–4]. In some cases, more than two trajectories approach the saddle point, creating a MB structure with a larger s-matrix size proportional to the number of trajectories. In this paper, we present a method to calculate the precise MB s matrix for any type of saddle point. It is based on rewriting the effective Hamiltonian in the Landau level basis, mapping the resulting algebraic problem to the 1D scattering in the quantum chain, and calculating the MB s matrix by properly fixing semiclassical modes in the far-away region.

As was found in the 1960s in pioneering works by Pippard [5–7], and Chambers [8–11], and summarized in Ref. [12], MB can lead to formation of coherent orbit networks composed of localized Landau level states (LLs) connected via tunneling between them. For 2D materials, the orbit network occurs in the vicinity of energy levels where the Bloch band in momentum space has saddle points located at the boundaries of the Brillouin zone (BZ). Then, tunneling between orbits in different cells of the extended BZ scheme forms a network (see Fig. 1). In the real space, this corresponds to a network of semiclassical cyclotron orbits, which makes LLs to be extended [5,8,12]. The discovery of novel 2D materials [13–16] dramatically increased the number of lattice geometries in which orbit networks can be formed. Below we calculate the detailed structure of these states as well as their band dispersion. In addition, we show that such extended LLs allow for longitudinal bulk conductance in the quantum Hall bar, which strongly exceeds the standard edge conductance [17].

There are two regimes of transport that orbit networks can govern: coherent regime with quantum phase that is accumulated along the cyclotron orbits and defines the exact energy spectrum, and incoherent regime with quantum phase averaged by the presence of disorder. Below, we describe the coherent regime and corresponding observable signatures that allow us to distinguish between different types of MB that happens at saddle points that connect cyclotron orbits. In addition, we note that the mini band structure appearing due to coherent orbit networks can be linked with the topological Hall effect of electrons in skyrmion crystals [22].

Recent studies of coherent orbit networks in 1D geometry predicted a number of interesting effects such as magic zeros in Landau level spectra [23] and broadening of the Landau levels by the coupling of Fermi arcs on opposite surfaces in Kramers-Weyl semimetals [24]. Also, the predicted spectrum by 2D incoherent orbit network shows relatively good agreement with the Hofstadter butterfly for twisted bilayer graphene [25]. The scaling of mini band width appearing from orbit networks with magnetic field was obtained for square lattice [26,27] and graphene [28].

The semiclassical equations of motion for the electron in crystal under external weak magnetic field are given by the Lorentz force [29,30]

$$\hbar \partial_t \boldsymbol{k} = -c^{-1} e (\boldsymbol{v}_k \times \boldsymbol{B}) \tag{1}$$

with usual velocity replaced by group velocity found from the dispersion law $\boldsymbol{v}_k = \frac{1}{\hbar}\partial_{\boldsymbol{k}} E(\boldsymbol{k})$ that depends on wave vector $\boldsymbol{k}$. Here, we consider 2D crystals placed in perpendicular magnetic field along the z-direction $\boldsymbol{B} = (0, 0, B)$. Equation (1)

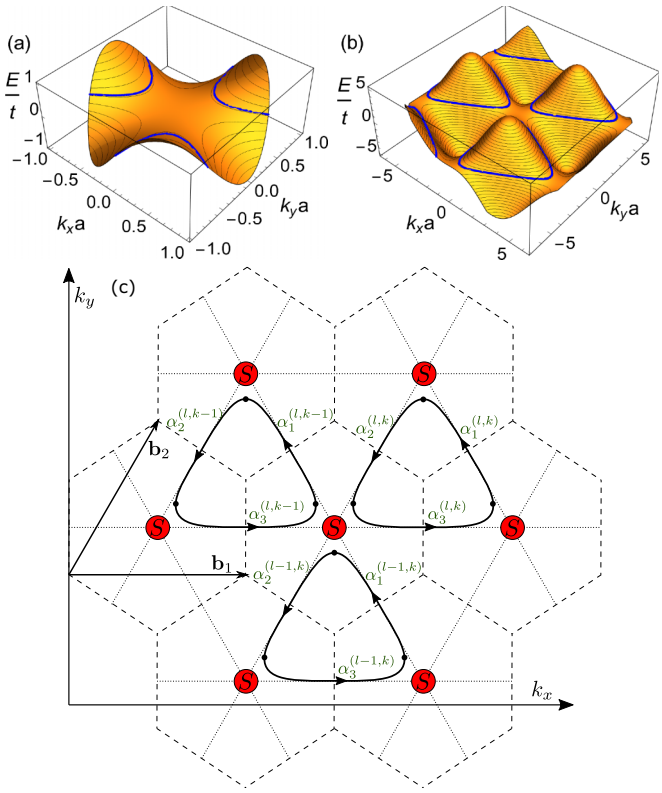

FIG. 1. (a) Effective dispersion around Monkey saddle point in momentum space given by Eq. (3) with three trajectories on a single energy level coming close at the MB region (shown as blue lines). (b) Tight-binding dispersion of triangular lattice with imaginary hoppings (18) in which monkey saddle points connect cyclotron orbits into network. (c) Planar orbit network for dispersion (b) in rotated coordinate frame with semiclassical regions labeled by weight coefficients α [see Eq. (14)], and MB regions with s matrix (red circles). Reciprocal lattice vectors $\boldsymbol{b}_i$ and highly symmetric lines are shown.

restricts quasiparticles to move only along the lines of constant energy in momentum space. In Fig. 1 such lines are shown in the vicinity of the monkey saddle point and in the dispersion of the tight-binding model introduced below in Eq. (18). Before proceeding to MB, we note that after integration over time in Eq. (1) one finds that the trajectory in real space is rotated by angle $\pi/2$ compared to the $E(\boldsymbol{k}) = \text{const}$ line in k space, and its size is rescaled by squared magnetic length [30,31]:

$$k_x = -\frac{y - y_0}{l_B^2}, \quad k_y = \frac{x - x_0}{l_B^2}, \quad l_B = \sqrt{\frac{\hbar c}{eB}}. \tag{2}$$

In what follows, we set $\hbar = c = 1$. Magnetic field is considered as weak if magnetic length is much larger than the lattice constant of the crystal, $l_b \gg a$.

We now focus on the detailed description of tunneling that takes place in the vicinity saddle point in dispersion due to magnetic breakdown. The saddle points are defined as points where the gradient of dispersion vanishes, $\nabla_{\boldsymbol{k}} E(\boldsymbol{k}) = 0$. As was shown in Ref. [2], they can be further classified as usual or high-order depending on the "flatness" of dispersion around that point. More formally, the usual type corresponds to nonvanishing determinant of Hessian matrix $\mathcal{D}_{ij} = \partial_{k_i}\partial_{k_j} E(\boldsymbol{k})$ for dispersion, while the high-order ones have zero determinant and optionally zero Hessian itself. They could be further classified into many types depending on the underlying symmetry point group, see Refs. [3,4]. Below, we show that our approach works for all possible saddle points. The magnetic breakdown happens because several constant energy lines in k-space come close to each other near the saddle point, see Fig. 1(a). Thus, the tunneling probability between them becomes of order of one, and therefore we have to properly solve the scattering problem in the corresponding region. The complication arises due to the fact that typical dispersion around the saddle point has high powers of polynomials in $\boldsymbol{k}$, for example

$$E_M(\boldsymbol{k}) = -ta^3\left(k_x^3 - 3k_x k_y^2\right) \tag{3}$$

for the monkey saddle. Here t is a constant with dimension of energy. Generally, it is not possible to solve a Schrödinger equation for such a Hamiltonian analytically to match it with plane-wave solutions away from the MB region. The only available closed form solution of such kind exists for the usual saddle point [18,20], a partial case of A_{2n-1} points,

$$E_{log}(\boldsymbol{k}) = ta^2\left(k_x^2 - k_y^2\right), \;\; E_{A_{2n-1}}(\boldsymbol{k}) = t\left(a^2 k_x^2 - (ak_y)^{2n}\right), \tag{4}$$

with $n = 1, 2, \ldots$. But we show that our seminumerical method efficiently solves the Schrödinger equation up to any precision and enables us to find the s matrix.

To introduce our method, we use the cylindrical gauge for vector potential $\boldsymbol{A} = \frac{B}{2}(-y, x, 0)$ and make use of the oscillator-type basis for Landau levels $|n\rangle$, with their coordinate representation given by

$$\psi_n(x, y) = \left(\frac{\partial}{\partial w} - \frac{w^*}{4l_B^2}\right)^n w^n e^{-|w|^2/4l_B^2}, \quad w = x + iy. \tag{5}$$

Using Landau level basis [32], the effective Hamiltonian of the saddle point in magnetic field that is written in terms of canonical momenta $\Pi_i = k_i + eA_i$ can be expressed in terms of ladder operators by using the replacement

$$k_x \to \Pi_x = \frac{\hat{a} + \hat{a}^\dagger}{\sqrt{2} l_B}, \; k_y \to \Pi_y = \frac{i(\hat{a} - \hat{a}^\dagger)}{\sqrt{2} l_B}, \tag{6}$$

with standard commutation relation $[\hat{a}, \hat{a}^\dagger] = 1$. In the simplest case of the usual saddle point, we find

$$H_{\log} = ta^2 l_B^{-2}[\hat{a}^2 + (\hat{a}^\dagger)^2]. \tag{7}$$

Here, we rescaled energy by t and set $l_B = a = 1$, which can be later restored by rescaling energy dependence of the s matrix. The more complicated example of monkey saddle (3) with mixed $k_x k_y^2$ product requires a symmetrization procedure to make the Hamiltonian Hermitian in terms of ladder operators. In the general case, different symmetrizations of particular polynomial Hamiltonian give different results for the lower order terms due to nontrivial commutation relations. To uniquely fix the symmetrization procedure, we expand the tight-binding Hamiltonian of the underlying lattice with assumption that momenta operators do not commute. For the Monkey saddle after simplification this reads [33]

$$H_M = -\frac{ta^3 l_B^{-3}}{2\sqrt{2}}[(\hat{a} + \hat{a}^\dagger)^3 + 3(\hat{a} - \hat{a}^\dagger)(\hat{a} + \hat{a}^\dagger)(\hat{a} - \hat{a}^\dagger)]. \tag{8}$$

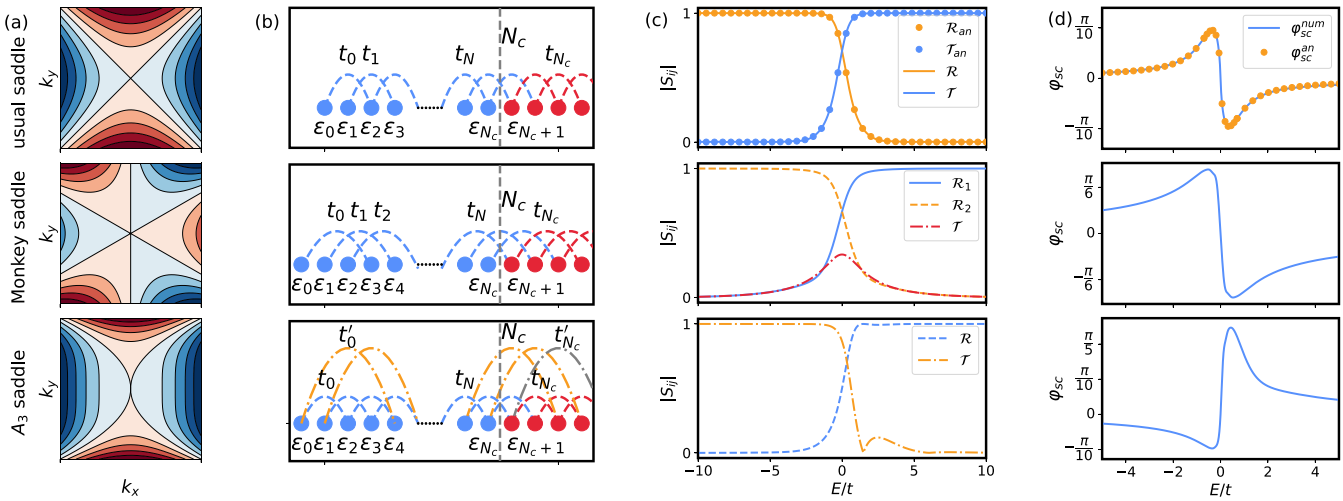

FIG. 2. (a) The geometry of usual, Monkey and A_3 saddle points with equi-energy contours in $k-$ space. (b): The corresponding 1D chains after mapping. The cut-off region with plane wave approximation is shown as a set of red sites with equal hopping parameters. (c) The absolute value of S-matrix elements (reflection - $\mathcal{R}_i$ and transmission - $\mathcal{T}$). (d): The basis-independent scattering phase calculated as arg(det[S]). For the usual saddle point (top panels in (c), (d)) we also show the comparison with exact analytic solution [18–20] marked by dots that perfectly agrees with the results obtained with our approach. In (c), (d) we set $l_B = 1$ and for any other magnetic field the results can be obtained by proper rescaling of energy [21].

We note that in more the general case of higher polynomial Hamiltonians one might find different symmetrization results depending on the lattice. If the tight-binding Hamiltonian is not known exactly, all possible symmetrizations that give different expressions in terms of ladder operators should be analyzed.

Next, we explain how to obtain the scattering matrix that describes magnetic breakdown around a saddle point. We start by noting that the exact solution of the Schödinger equation $H\Psi = E\Psi$ with $\Psi = \sum_{n=0}^{\infty}\phi_n|n\rangle$ yields a set of recursive equations. For a usual van Hove singularity, we find

$$E\varphi_0 - \sqrt{2}\phi_2 = 0, \quad E\phi_1 - \sqrt{6}\phi_3 = 0,$$
$$E\phi_n - \sqrt{n(n-1)}\phi_{n-2} - \sqrt{(n+1)(n+2)}\phi_{n+2} = 0. \quad (9)$$

Recursive equations for other saddle points are derived in the Supplemental Material [33]. We note that a set of recursive equations can be mapped onto a 1D tight-binding problem: the term multiplying φ_n corresponds to an on-site potential for the site with index n, while the terms involving φ_m with $m \neq n$ represent the tight-binding hopping parameters that connect the nth site to the mth site. By imposing truncation at large index $n = N_c$ and replacing all remaining equation with those where $n = N_c$, we obtain a natural mapping to N_c-site 1D chain of atoms connected to a translationally invariant semiinfinite lead, shown in Fig. 2(b). Then, we obtain the s matrix using the propagating modes of the lead at energy E, with the number of scattering states corresponding to the number of semiclassical orbits coming close at the MB region.

However, the obtained s matrix is in the LL basis. To transform the s matrix into basis of modes with a definite angle in momentum space, we use the creation ladder operator

$$a^\dagger \sim k_x + ik_y \equiv ke^{i\phi_k}, \quad (10)$$

where ϕ_k is the angle in momentum space. Hence, performing a basis transformation on the propagating modes in semiinfinite leads to a basis where $a^\dagger$ is diagonal and converts the obtained s matrix into a physical one. The technical details of this procedure for the usual and Monkey saddle are discussed in the Supplemental Material [33]. The chirality and consequent absence of backscattering of the states with definite angle, that are spatially separated, ensures the unique definition of the physical s matrix.

For some saddle points the asymptotic modes at large momenta are indistinguishable by their angle in momentum space. In this case, we cannot apply our procedure of transforming the s matrix into a physical basis. An example of such a saddle point is A_{2n-1} described by Eq. (4). For this saddle point, the angle of trajectory in momentum space with respect to the x axis tends to zero as the wave number tends to infinity, see the bottom panel of Fig. 2(a). We resolve this by introducing angle-fixing regularization, achieved through the inclusion of sufficient amount of subleading terms in the effective Hamiltonian

$$E'_{A_{2n-1}}(\boldsymbol{k}) = t\left(a^2k_x^2 - a^{2n}\left(k_y^{2n} - \beta k_x^{2n}\right)\right), \; n \geqslant 2, \quad (11)$$

where we use the $\beta > 0$ constant as a regularization parameter and this parameter defines angles far away from the scattering region, not playing a role in the vicinity of the saddle point. We choose the truncation number N_c such that the leading terms strongly dominate in effective 1D tight-binding equations, and the mode separation into the angle basis can be done with good precision: $t_{N_c+1}^{\max} \gg E, \ldots$. Physically, this corresponds to taking the region where the scattering between modes with different angles is absent.

To demonstrate our method, we numerically solve for the scattering matrix using Kwant code [34,35]. We show our results for the absolute values of the transmission and reflection elements of the s matrix and scattering phases in panels (c) and (d) of Fig. 2. All these elements are gauge invariant and independent of incoming and outgoing basis modes selection.

In the case of usual van Hove singularity, it demonstrates perfect agreement with analytic expressions (see [20,33]). For the A_3 saddle point, we find a nontrivial behavior of transmission coefficients shown in bottom row in Fig. 2(c). The presence of zeros in the transmission coefficient signifies the complete reflection of a quasiparticle moving along a cyclotron trajectory at that specific energy. Consequently, this phenomenon results in the effective reduction of orbit network to a single cell. The manifestation of this effect is demonstrated below by the narrowing of the mini band width in the spectrum and the corresponding reduction in bulk conductance. With the complete description of MB at hand, we now propose a transport setup which would probe the features of the high-order saddle points. Since our goal is to distinguish energy dependence of both scattering amplitude and phase of MB at different saddle points, we use the coherent orbit networks that appear when the saddle points are placed at the edge of the BZ. Such coherent orbit networks were widely discussed in literature in the late 1960s [5,8,12], but the absence of experiments with 2D atomically thin crystals limited discussion to the simplest geometries, such as weak perturbative potential with square lattice geometry. Here, we use the same approach of magnetic translation symmetry groups and describe the orbit networks that are connected via usual as well as high-order saddle points. As it is clear from the constant energy curves in the spectrum in the extended BZ scheme [see Fig. 1(b)], the orbits networks in k space have perfect periodicity and thus should be periodic in r space. However, in the presence of external magnetic field, the translation operators of the lattice $\hat{T}_{\boldsymbol{R}_i} = \exp\{\nabla_r \boldsymbol{R}_i\}$, with $\boldsymbol{R}_i$ being a basis vector, should be replaced by magnetic translation operators [12], which up to phase factor are equal to $\hat{T}^M_{\boldsymbol{R}_i} = \exp\{(\nabla_r + ie(\boldsymbol{A}(\boldsymbol{R}_i) + \boldsymbol{R}_i \times \boldsymbol{B}))\boldsymbol{R}_i\}$. The corresponding operators define a magnetic unit cell. To obtain a closed set of equations for the orbit network, we should restrict the value of magnetic flux per unit cell of the lattice to be a rational number

$$\Phi = B|\mathbf{R}_1 \times \mathbf{R}_2| = B\frac{(2\pi)^2}{|\mathbf{b}_1 \times \mathbf{b}_2|} = \frac{q}{p}\Phi_0, \quad \Phi_0 = \frac{h}{e}. \tag{12}$$

Here, $\boldsymbol{b}_i$ are the basis vectors of reciprocal lattice. In the further calculations, we restrict ourselves to the case of $q = 1$. This relation is equivalent to setting magnetic unit cell to the integer number p of lattice unit cells. Now we are ready to proceed with defining a basis of semiclassical wave functions on the links of networks. These are Zilberman-Fischbeck (ZF) wave functions [12,20,36], written using the WKB-type approximation far from scattering region. The ZF functions are expressed in a gauge-invariant coordinate space with replacement $\Pi_x \to k_x$ and $\Pi_y \to -il_B^{-2}\partial_{k_x}$. Since the scope of this paper is limited by the linear effects in magnetic field, we use the first order expansion of ZF functions with $a^2/l_B^2 \ll 1$:

$$\Psi_{ZF}(k_x) = \left|\frac{\partial E(\boldsymbol{k})}{\partial k_y(k_x)}\right|^{-\frac{1}{2}} \exp\left[-il_B^2\int_{k_{x,0}}^{k_x} k_y^E(k_x)\,dk_x\right]. \tag{13}$$

Here $k_y^E(k_x)$ stands for the solution of constant energy contour equation $E(k_x, k_y^E(k_x)) = E$. The full wave function of the orbit network state is composed as a weighted superposition of the Ψ_{ZF} wave functions in different unit cells:

$$\Psi(k_x) = \sum_{k,l}^{\infty} e^{il_B^2[k_x l b_{2,y} - \frac{l^2}{2} b_{2,x} b_{2,y}]} \times \sum_j \alpha_j^{(l,k)} \Psi_{ZF}^j(k_x - kb_{1,x} - lb_{2,x}). \tag{14}$$

In this expression, each weight coefficient $\alpha_j^{(l,k)}$ contains two cell indices l, k as well as a unique index j corresponding to the different parts of the orbit between scattering points inside single cell of the network. The example of this notation is shown in Fig. 1. Due to periodicity of the network, the solutions have the form of Bloch waves $\alpha_j^{(l,k)} = \alpha_j e^{i(p_k k + p_l l)}$. The magnetic translation group restricts the allowed values of $p_{l,k}$ to particular dependence on translation operator $\hat{T}^M_{\boldsymbol{R}_i}$ eigenvalues $\boldsymbol{q}$: $p_l = -l_B^2(q_x b_{2,y} - q_y b_{2,x})$, $p_k = l_B^2 q_y K_{1,x}$ [33]. Next, we use the s matrices obtained above to couple the ZF solutions in the neighboring cells. By noting that ZF functions from Eq. (13) correspond to the modes with proper angles, we can straightforwardly insert parameters of the s matrix into the system of equations, and write it in the form of a Ho-Chalker operator [37]:

$$\hat{S}_{HC}(E, \boldsymbol{q})\boldsymbol{\alpha} = 0. \tag{15}$$

While substituting the s matrix, we subtracted the difference in dynamical phases of modes with defined angles and ZF functions (13) at given energy. Such a difference appears due to the fact that in geometry of the scattering problem one assumes semiclassical ZF solutions with the phase fixed at infinity, while in the orbit network ZF function phase is fixed at particular point inside the network unit cell.

The nonlinear eigenvalue problem for the Ho-Chalker operator (15) can be rewritten in the form of spectral equation $\det \hat{S}_{HS}(E, \mathbf{q}) = 0$ for a given lattice model [33]. Below we demonstrate this for square and triangular lattice, and show that the MB s matrix calculated above plays a key role in definition of the properties of coherent orbit network. In the case of square lattice with only first and third NN hoppings taken into account,

$$H_{sq}(\boldsymbol{k}) = -2\sum_{i=x,y}(t\cos k_i a + t_3 \cos 2k_i a), \tag{16}$$

the spectral equation is

$$\cos\left(\frac{l_B^2\mathcal{A}(E)}{2} - \varphi_{sc}\right) = \pm\mathcal{T}\mathcal{R}\left[\cos\left(l_B^2 q_1 b_{2,y}\right) + \cos\left(l_B^2 q_2 b_{1,x}\right)\right]. \tag{17}$$

Here, $\mathcal{A}(E)$ is the area enclosed by the constant energy curve in momentum space. The elements of the s matrix, denoted as $\mathcal{R}$ reflection, $\mathcal{T}$ transmission, and $\varphi_{sc} = \arg(\det S)$ is the scattering phase, are shown in Fig. 2. For such a lattice Hamiltonian, the connection of orbits happens via usual van Hove singularity at the x point of BZ for $t_3 = 0$ or via high-order van Hove singularity of A_3 type for $t_3 = t/4$. In the case of the

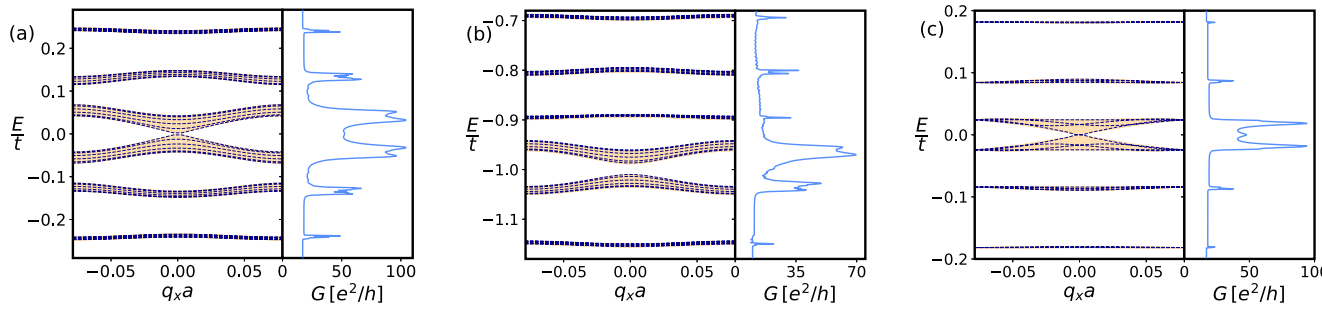

FIG. 3. Comparison of Landau mini band spectrum with longitudinal conductance in the quantum Hall bar for three systems: (a), (b) square lattice with usual [hopping $t_2 = 0$ in Eq. (16)] and A_3 ($t_2 = t/4$) saddle points, and (c) triangular lattice with imaginary hoppings that contain Monkey saddles. LL mini bands (orange solid lines) obtained from tight-binding simulations are compared with solutions of spectral equations (17), (19) for a set of $q_y a$ (blue dashed lines). The flux value per unit cell was taken equal to $\Phi = 1/40\,\Phi_0$ and the width of the Hall bar was $W = 320a$. For the spectrum calculation a periodic boundary condition was imposed. A single period of Landau mini band oscillation is shown and corresponds to $\sqrt{\Phi/\Phi_0}$ part of BZ. The width of conductance peaks measures the Landau mini band broadening. In panel (b) the mini band around $E \approx -0.8t$ is wider than the one at $E \approx -0.9t$ due to the first zero of transmission coefficient at the A_3 saddle point (see Fig. 2(c) [21]).

triangular lattice with imaginary hoppings, the dispersion is

$$H_{tr}(\mathbf{k}) = 2t\left(\sin k_x a - \sin\frac{k_x - \sqrt{3}k_y}{2}a - \sin\frac{k_x + \sqrt{3}k_y}{2}a\right). \tag{18}$$

The monkey saddle (see Fig. 1) connects orbits from different cells into a network. The corresponding spectral equation is

$$\begin{aligned}\cos\left(\frac{l_B^2\mathcal{A}(E) - \varphi_{sc}}{2}\right) = \mathcal{T}\Bigg[&\cos\left(l_B^2 q_2 b_{1,x} - \frac{\pi p}{2}\right)\\ &+ \cos\left(l_B^2[q_1 b_{2,y} + q_2(b_{1,x} - b_{2,x})] - \frac{\pi p}{2}\right)\\ &+ \cos\left(l_B^2[q_1 b_{2,y} - q_2 b_{2,x}] - \frac{\pi p}{2}\right)\Bigg].\end{aligned} \tag{19}$$

The left-hand side of each spectral equation, as defined in (17) and (19), yields the conventional flat Landau levels when equated to zero. On the other hand, the nonzero right-hand side converts Landau levels into mini bands. The width of these mini bands is determined by the van Hove singularity, the s-matrix transmission coefficient, and the lattice-specific dispersion. To explore this behavior, we numerically solve [35] the spectral equations for different values of q_x and for a small set of q_y. The resulting mini band structures are depicted by the blue dashed lines in Fig. 3, showing both the width and internal structure of analytic spectrum of a mini band. The spectrum obtained from a tight-binding simulation [34,35] is shown as orange lines filling the corresponding regions and demonstrates excellent agreement with the semiclassical predictions. For our analysis, we utilized a narrow Hall bar geometry with periodic boundary conditions, having a width several times larger than the magnetic unit cell. That width is already enough to have many bulk conducting states inside the orbit network.

The appearance of oscillating dispersion and broadening of Landau levels due to orbit networks is expected to be manifested in the transport experiments such as Shubnikov-de-Haas oscillations or high-frequency magnetic breakdown oscillations [24,38–42]. As the most pronounced signature, we present a calculation of longitudinal conductance in two-terminal Hall bar geometry. Typically, such conductance is governed by edge states [17] and is strongly suppressed. As it is shown in the right part of each panel in Fig. 3, the dispersive Landau mini bands induce bulk conductance that is much larger than background edge conductance. We compared the spectrum for the lattices with periodic boundary condition with the conductance shape in finite size systems for the same values of magnetic field. The width of the peaks in the conductance agrees with the broadening of Landau mini bands, thus providing a tool for estimation of the tunneling probabilities $\mathcal{T}$ for MB s matrix at the saddle point. In addition, we note that the specific property of the A_3 saddle point with zero transmission coefficient [see Fig. 2(c)] leads to a much smaller conductance peak at corresponding chemical potential compared to other peaks, shown in Fig. 3(b).

To give an estimate of magnetic field required for the experiment, we use an estimate of magnetic length $l_B \approx 26\,\mathrm{nm}/\sqrt{B[T]}$ with typical experimental values of magnetic field $B \sim 10\,T$ [43], which gives $l_B \approx 10\,\mathrm{nm}$. The broadening of the Landau mini band becomes significant compared to the hopping parameter (see Fig. 3) and larger than disorder broadening for magnetic fluxes around $\Phi = 10^{-2}\Phi_0$ per lattice unit cell. Thus, it requires lattice constant to be of the order of $a \sim l_B\sqrt{2\pi\,\Phi/\Phi_0} \sim 2.5\,\mathrm{nm}$. Such an estimate shows that one requires extremely high magnetic field to measure such effects in conventional systems, such as highly doped monolayer graphene [44]. But, such lattice constants are typical for the modern artificial lattices [45] as well as for Moiré materials such as twisted bilayer graphene [46–48]. In addition, we point out that the method of solving the MB problem developed above can be applied for the systems with spin-orbit coupling, such as Moiré bilayer transition-metal dichalcogenides [49]. The structure of the orbit network might be visualized by injecting the current at proper chemical potential levels into the system via narrow lead. The picture of current density distribution is expected to follow the pattern of orbit network shown in Fig. 1 and might be probed by STM-type microscopy techniques [50,51].

We are grateful to C. Beenakker, G. Lemut, J. Tworzydlo, M. Katsnelson, M. Pacholski, and J. Zijderveld for fruitful discussions. A part of code is written for the Kwant package [34] by J. B. Weston and T. Ö. Rosdahl. V.A.Z. and D.O.O. acknowledge the support from the Netherlands Organization for Scientific Research (NWO/OCW) and from the European Research Council (ERC) under the European Union's Horizon 2020 research and innovation programme. A.M.B. acknowledges the NWO Grant No. OCENW.GROOT.2019.004. A.R.A. acknowledges the NWO VIDI Grant No. (016.Vidi.189.180). V.A.Z. performed the analytical calculations and numerical tight-binding simulations for orbit networks. A.M.B. performed numerical calculations for scattering matrices and contributed to tight-binding simulations. A.R.A. formulated the idea of ladder operator approach for *s*-matrix calculation. D.O.O. organized the workflow, wrote the manuscript, and helped with analytical calculations and tight-binding simulations. All authors contributed to reviewing and editing the manuscript.

[1] L. Van Hove, The occurrence of singularities in the elastic frequency distribution of a crystal, Phys. Rev. **89**, 1189 (1953).

[2] N. F. Q. Yuan, H. Isobe, and L. Fu, Magic of high-order van Hove singularity, Nat. Commun. **10**, 5769 (2019).

[3] A. Chandrasekaran, A. Shtyk, J. J. Betouras, and C. Chamon, Catastrophe theory classification of fermi surface topological transitions in two dimensions, Phys. Rev. Res. **2**, 013355 (2020).

[4] N. F. Q. Yuan and L. Fu, Classification of critical points in energy bands based on topology, scaling, and symmetry, Phys. Rev. B **101**, 125120 (2020).

[5] A. B. Pippard, Quantization of coupled orbits in metals, Proc. R. Soc. London A **270**, 1 (1962).

[6] A. B. Pippard, Quantization of coupled orbits in metals II. the two-dimensional network, with special reference to the properties of zinc, Philos. Trans. Roy. Soc. A **256**, 317 (1964).

[7] A. B. Pippard, Magnetic breakdown in a dislocated lattice, Proc. R. Soc. London A **287**, 165 (1965).

[8] W. G. Chambers, Linear-network model for magnetic breakdown in two dimensions, Phys. Rev. **140**, A135 (1965).

[9] W. G. Chambers, Magnetic breakdown: Effective hamiltonian and de haas-van alphen effect, Phys. Rev. **149**, 493 (1966).

[10] W. G. Chambers, Magnetic breakdown and oscillatory magnetoresistance by a kubo formula, Phys. Rev. **165**, 799 (1968).

[11] W. G. Chambers, Oscillatory magnetoconductivity in a linear chain of orbits coupled by magnetic breakdown, J. Phys. F **3**, 1216 (1973).

[12] H. J. Fischbeck, Theory of bloch electrons in a magnetic field, physica status solidi (b) **38**, 11 (1970).

[13] K. S. Novoselov, A. K. Geim, S. V. Morozov, D. Jiang, Y. Zhang, S. V. Dubonos, I. V. Grigorieva, and A. A. Firsov, Electric field effect in atomically thin carbon films, Science **306**, 666 (2004).

[14] K. S. Novoselov, D. Jiang, F. Schedin, T. J. Booth, V. V. Khotkevich, S. V. Morozov, and A. K. Geim, Two-dimensional atomic crystals, Proc. Natl. Acad. Sci. USA **102**, 10451 (2005).

[15] K. S. Novoselov, A. Mishchenko, A. Carvalho, and A. H. Castro Neto, 2D materials and van der Waals heterostructures, Science **353**, aac9439 (2016).

[16] S. Manzeli, D. Ovchinnikov, D. Pasquier, O. V. Yazyev, and A. Kis, 2d transition metal dichalcogenides, Nat. Rev. Mater. **2**, 17033 (2017).

[17] *The Quantum Hall Effect*, edited by R. E. Prange and S. M. Girvin (Springer, New York, 1990).

[18] M. Y. Azbel, Quasiclassical quantization in the neighborhood of singular classical trajectories, Sov. Phys. JETP **12**, 891 (1961).

[19] M. Y. Azbel, Energy spectrum of a conduction electron in a magnetic field, Sov. Phys. JETP **19**, 634 (1964).

[20] A. Alexandradinata and L. Glazman, Semiclassical theory of Landau levels and magnetic breakdown in topological metals, Phys. Rev. B **97**, 144422 (2018).

[21] For the Hamiltonian written in gauge-invariant coordinates $H = A\Pi_x^n + B\Pi_x^s\Pi_y^m = Ak_x^n + Bk_x^s(-\frac{i}{l_B^2}\frac{\partial}{\partial k_x})^m$ it is possible to introduce a change of variables $q_x = k_x l_B^{\frac{2m}{m+n-s}}$, that would convert it to $l_B = 1$ Hamiltonian with additional factor $H = l_B^{\frac{2mn}{m+n-s}}[Aq_x^n + Bq_x^s(-i\frac{\partial}{\partial q_x})^m]$. This factor should be used to obtain energy dependence of S-matrix for any magnetic field value.

[22] B. Göbel, A. Mook, J. Henk, and I. Mertig, Signatures of lattice geometry in quantum and topological Hall effect, New J. Phys. **19**, 063042 (2017).

[23] N. Paul, P. J. D. Crowley, T. Devakul, and L. Fu, Moiré Landau fans and magic zeros, Phys. Rev. Lett. **129**, 116804 (2022).

[24] G. Lemut, A. D. Vela, M. J. Pacholski, J. Tworzydło, and C. W. J. Beenakker, Magnetic breakdown spectrum of a kramers–weyl semimetal, New J. Phys. **22**, 093022 (2020).

[25] C.-K. Lu and H. A. Fertig, Magnetic breakdown in twisted bilayer graphene, Phys. Rev. B **89**, 085408 (2014).

[26] V. M. Gvozdikov and M. Taut, Magnetic quantum oscillations of electrons on a two-dimensional lattice: Numerical simulations and the magnetic breakdown approach, Phys. Rev. B **75**, 155436 (2007).

[27] A. Nikolaev and M. Zhuravlev, Anomalous broadening of Landau levels at the saddle point energy of two dimensional square lattice, J. Magn. Magn. Mater. **560**, 169674 (2022).

[28] A. V. Nikolaev, Saddle point anomaly of landau levels in graphenelike structures, Phys. Rev. B **104**, 035419 (2021).

[29] A. B. Pippard, Experimental analysis of the electronic structure of metals, Rep. Prog. Phys. **23**, 176 (1960).

[30] I. M. Lifshitz and M. I. Kaganov, Some problems of the electron theory of metals I. Classical and quantum mechanics of electrons in metals, Sov. Phys. Usp. **2**, 831 (1960).

[31] R. Stark and L. Falicov, Chapter VI magnetic breakdown in metals, in *Progress in Low Temperature Physics*, edited by C. J. Gorter (John Wiley and Sons, Hoboken, NJ, 1967), pp. 235–286.

[32] We note that we take Landau basis with $m_z = 0$. For the problems in empty space different m_z states are trivially degenerate. The problem at hand does not mix different m_z states.

[33] See Supplemental Material at http://link.aps.org/supplemental/10.1103/PhysRevB.109.L081103 for technical details of map-

ping the MB problem to scattering in 1D chains and derivation of orbit network spectral equations for square and triangular lattice.

[34] C. W. Groth, M. Wimmer, A. R. Akhmerov, and X. Waintal, Kwant: A software package for quantum transport, New J. Phys. **16**, 063065 (2014).

[35] V. Zakharov, A. M. Bozkurt, A. R. Akhmerov, and D. O. Oriekhov, Code for "Landau quantization near generalized van Hove singularities: magnetic breakdown and orbit networks" (2023), 10.5281/zenodo.7707909.

[36] G. E. Zil'berman, Behavior of an electron in a periodic electric and a uniform magnetic field, Sov. Phys. JETP **5**, 208 (1957).

[37] C.-M. Ho and J. T. Chalker, Models for the integer quantum Hall effect: The network model, the Dirac equation, and a tight-binding Hamiltonian, Phys. Rev. B **54**, 8708 (1996).

[38] R. R. Gerhardts, D. Weiss, and K. v. Klitzing, Novel magnetoresistance oscillations in a periodically modulated two-dimensional electron gas, Phys. Rev. Lett. **62**, 1173 (1989).

[39] R. W. Winkler, J. P. Kotthaus, and K. Ploog, Landau band conductivity in a two-dimensional electron system modulated by an artificial one-dimensional superlattice potential, Phys. Rev. Lett. **62**, 1177 (1989).

[40] C. W. J. Beenakker, Guiding-center-drift resonance in a periodically modulated two-dimensional electron gas, Phys. Rev. Lett. **62**, 2020 (1989).

[41] P. Streda and A. H. MacDonald, Magnetic breakdown and magnetoresistance oscillations in a periodically modulated two-dimensional electron gas, Phys. Rev. B **41**, 11892 (1990).

[42] V. M. Gvozdikov, Magnetoresistance oscillations in a periodically modulated two-dimensional electron gas: The magnetic-breakdown approach, Phys. Rev. B **75**, 115106 (2007).

[43] J. Finney, A. L. Sharpe, E. J. Fox, C. L. Hsueh, D. E. Parker, M. Yankowitz, S. Chen, K. Watanabe, T. Taniguchi, C. R. Dean, A. Vishwanath, M. A. Kastner, and D. Goldhaber-Gordon, Unusual magnetotransport in twisted bilayer graphene, Proc. Natl. Acad. Sci. USA **119**, e2118482119 (2022).

[44] P. Rosenzweig, H. Karakachian, D. Marchenko, K. Küster, and U. Starke, Overdoping graphene beyond the van Hove singularity, Phys. Rev. Lett. **125**, 176403 (2020).

[45] M. R. Slot, T. S. Gardenier, P. H. Jacobse, G. C. P. van Miert, S. N. Kempkes, S. J. M. Zevenhuizen, C. M. Smith, D. Vanmaekelbergh, and I. Swart, Experimental realization and characterization of an electronic Lieb lattice, Nat. Phys. **13**, 672 (2017).

[46] K. Kim, A. DaSilva, S. Huang, B. Fallahazad, S. Larentis, T. Taniguchi, K. Watanabe, B. J. LeRoy, A. H. MacDonald, and E. Tutuc, Tunable moiré bands and strong correlations in small-twist-angle bilayer graphene, Proc. Natl. Acad. Sci. USA **114**, 3364 (2017).

[47] Y. Cao, V. Fatemi, S. Fang, K. Watanabe, T. Taniguchi, E. Kaxiras, and P. Jarillo-Herrero, Unconventional superconductivity in magic-angle graphene superlattices, Nature (London) **556**, 43 (2018).

[48] Y. Kim, P. Moon, K. Watanabe, T. Taniguchi, and J. H. Smet, Odd integer quantum hall states with interlayer coherence in twisted bilayer graphene, Nano Lett. **21**, 4249 (2021).

[49] Y.-T. Hsu, F. Wu, and S. Das Sarma, Spin-valley locked instabilities in moiré transition metal dichalcogenides with conventional and higher-order van Hove singularities, Phys. Rev. B **104**, 195134 (2021).

[50] E. Y. Andrei, G. Li, and X. Du, Electronic properties of graphene: A perspective from scanning tunneling microscopy and magnetotransport, Rep. Prog. Phys. **75**, 056501 (2012).

[51] Y. Xie, B. Lian, B. Jäck, X. Liu, C.-L. Chiu, K. Watanabe, T. Taniguchi, B. A. Bernevig, and A. Yazdani, Spectroscopic signatures of many-body correlations in magic-angle twisted bilayer graphene, Nature (London) **572**, 101 (2019).